



Electrochemical performance of a tin-coated carbon fibre electrode for rechargeable lithium-ion batteries

Mehdi Shafiei*, Ahmet T. Alpas

Department of Mechanical, Automotive and Materials Engineering, University of Windsor, 401 Sunset Avenue, Windsor, Ontario N9B 3P4, Canada

ARTICLE INFO

Article history:

Received 5 February 2011

Received in revised form 21 April 2011

Accepted 22 April 2011

Available online 30 April 2011

Keywords:

Lithium-ion battery

Composite anode

Electrodeposition

Ultrafine grain tin

Carbon fibre

ABSTRACT

An Sn–carbon fibre composite electrode is fabricated by electrodepositing a thin film ($0.5 \pm 0.1 \mu\text{m}$) of Sn with an ultrafine grain size ($350 \pm 50 \text{ nm}$) on the $7.5 \pm 1.5 \mu\text{m}$ diameter fibres of a carbon fibre paper (CFP). The electrochemical performance of the Sn–CFP composite being considered as an anode material for rechargeable Li-ion batteries is evaluated by conducting galvanostatic charge–discharge cycling tests. The Sn–CFP electrode displays a reversible planar capacity of 2.96 mAh cm^{-2} with a capacity retention of 50% after twenty cycles, compared to the 23% measured for a $2.2 \pm 0.2 \mu\text{m}$ thick Sn coating deposited on a Cu foil. The enhanced cycling performance of the Sn–CFP electrode is attributed to the double role played by carbon fibres, which act as randomly oriented current collectors in addition to being an active material. The small thickness and large surface area of the Sn coating on the carbon fibres enhances the coating's chemical reactivity and tolerance for volume change. It is suggested that transforming Sn to Sn oxides in Sn–CFP electrodes may improve the cycling performance of these composites as anode materials for rechargeable Li-ion batteries.

© 2011 Elsevier B.V. All rights reserved.

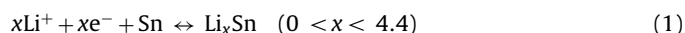
1. Introduction

The most common anode material used in Li-ion batteries is graphite, due to its low cost, availability and durability [1,2]. In graphitic anodes, the Li^+ insertion mechanism corresponds to the reversible, progressive intercalation of Li^+ ions between graphene layers to reach a theoretical capacity of 372 mAh g^{-1} if LiC_6 is formed [3], compared to a practical capacity of 350 mAh g^{-1} [4].

Recent years have seen a growing interest in the use of affordably mass-producible metals (e.g., Si, Sn, Sb, In, Bi, Al) as Li-ion battery anode materials to achieve a higher capacity and a more positive lithiation voltage vs. Li/Li^+ , minimizing the risk of Li plating that is a safety problem with carbonaceous anodes [4,5]. However, using the aforementioned metals as anodes for Li-ion batteries produces large volume changes during lithiation/delithiation processes. Thus, in order to improve durability while maintaining high capacity, new strategies have been implemented to prevent the adverse effects of large volume changes. One strategy is the development of intermetallic anode materials by alloying active elements with inactive elements (e.g., Cu_6Sn_5 , Cu_2Sb) to compensate for the expansion of the active materials [6,7]. Another strategy employed by some researchers is the development of composite anode materials by mixing active elements with carbonaceous materials (e.g., Si–C, Sn–C) [8,9] or oxides (e.g., Sb– VO_4 ,

Sb– Mn_2O_7 , Sn– Al_2O_3) [10,11]. For example, Magasinski et al. [8] used a CVD technique to produce Si–C nanocomposite granules containing 50 wt% Si nanoparticles, and reported a capacity of 1500 mAh g^{-1} with an efficiency of about 90% for 100 cycles. A third strategy involves the design and development of anode materials with micro- and nano-scale surface textures that provide a large surface-to-volume ratio. This may result in an improvement of the electrical contact between the active material and the current collector, an enhancement of the chemical reactivity of the active material to the electrolyte, and an increase in the tolerance for the volume change [8,12,13].

Among the alternative anode materials that have been studied, Sn is particularly important because of its high theoretical capacity of 992 mAh g^{-1} (i.e., if $\text{Li}_{4.4}\text{Sn}$ is reached) [14–17]. The Li^+ insertion mechanism in Sn-based anodes corresponds to the formation of Li–Sn intermetallics according to:



Sn has a poor capacity retention, however, due to its large volume change (up to 300%) during charge–discharge cycles, which causes the pulverization of the electrode after only a few cycles [14–17]. In order to improve the cycling performance of Sn anodes, Sn-based intermetallic compounds and composite materials have been developed. Intermetallics formed of Sn and inactive elements, such as Cu_6Sn_5 [18–20], CoSn_3 [21] and Ni_3Sn_4 [22–24], have a lower specific capacity than pure Sn, but their capacity retention is significantly higher.

* Corresponding author. Tel.: +1 5192533000x2603; fax: +1 5199737085.
E-mail address: shafiei@uwindsor.ca (M. Shafiei).

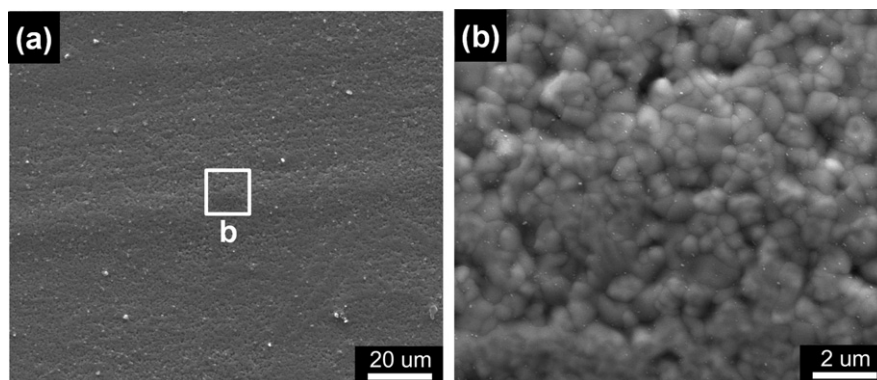


Fig. 1. SEM (secondary electron) micrographs of the Sn coating electrodeposited on a Cu foil current collector.

There are also several examples of Sn-based composite anodes in the literature. Noh et al. [25] produced amorphous carbon-coated Sn particles composed of 80 wt% Sn. Testing a composite electrode with 60 wt% particles, they measured a capacity of 680 mAh g^{-1} and a capacity retention of 98% after 50 cycles. Park et al. [26] showed that the cycling performance of electrodeposited Sn coatings could be improved by dispersing 16 vol% acetylene black particles with a size smaller than $40 \mu\text{m}$ into the Sn matrix. They reported a capacity of 460 mAh g^{-1} and a capacity retention of 43% after twenty cycles for the composite electrode, whereas a similar $10 \mu\text{m}$ -thick Sn coating showed a small capacity of only 20 mAh g^{-1} from the beginning. This improvement in the cycling performance was attributed to the buffering effect that the acetylene black particles had on the volume change. On the other hand, the use of three-dimensional substrates (current collectors) for Sn-based coatings like metallic foams [27–29], nanopillar-textured Cu surface [30] and carbon fibre

paper (CFP) [31], have also shown to improve the durability of the anode electrodes. Among these, using CFP seems to be the simplest, most cost-effective approach, because it does not require adding extra steps to the electrode production route.

The aim of this study was to fabricate an Sn–carbon fibre composite as an alternative (with higher capacity and improved safety) to commercial graphitic anodes for rechargeable Li-ion batteries using a cost-effective electrodeposition process. Galvanostatic charge–discharge cycling tests would then be conducted to evaluate the electrode's reversible capacity and cycling performance with the goal of understanding the roles that Sn and carbon fibres play in the overall performance of these composite anodes. Furthermore, the microstructures of the electrodes were studied to understand the electrochemical degradation mechanisms and suggest possible materials processing solutions that might improve the performance of the composite electrodes.

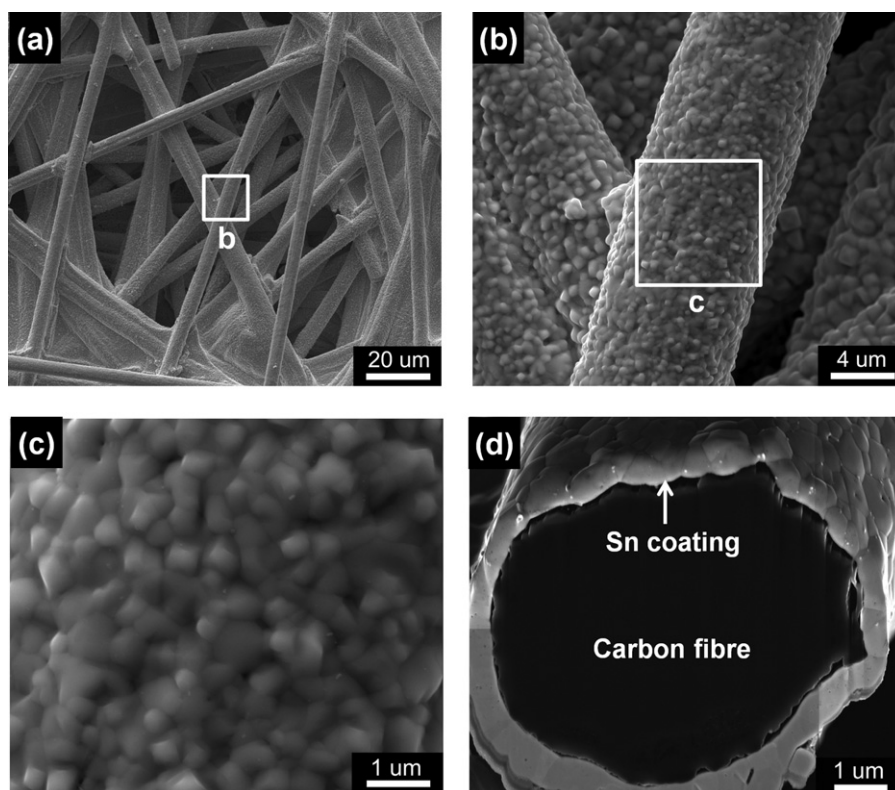


Fig. 2. SEM (secondary electron) micrographs of the Sn–CFP electrode: (a) Sn–CFP microstructure, (b) Sn-coated carbon fibres in the electrode, (c) surface morphology of the Sn coating on a carbon fibre showing the Sn ultrafine grain structure, and (d) an FIB-milled cross section of an Sn-coated carbon fibre.

To fabricate the composite electrode, a thin film of ultrafine grain Sn (it has been suggested that a reduction in the active material's grain size may benefit the cycling performance by reducing crack size and delamination from the current collector during charge–discharge cycles [14]) was electrodeposited on a CFP sheet with randomly oriented carbon fibres. CFP is low-cost and commercially available, and it has a large surface area and good electrical conductivity. The electrochemical performance and the degradation mechanisms of this electrode were compared to an Sn coating electrodeposited on a Cu foil.

2. Experimental

2.1. Fabrication and characterization of electrodes

A thin layer of Sn with a mass loading of $3.2 \pm 0.2 \text{ mg cm}^{-2}$ was electrodeposited on the randomly oriented, $7.5 \pm 1.5 \text{ }\mu\text{m}$ diameter fibres of a 0.37 mm thick Toray CFP sheet with a specific mass of $16.2 \pm 0.2 \text{ mg cm}^{-2}$ and a porosity of 78%. A pyrophosphate bath containing 0.40 M $\text{K}_4\text{P}_2\text{O}_7$, 0.09 M $\text{Sn}_2\text{P}_2\text{O}_7$ and 0.05 M $\text{C}_4\text{H}_6\text{O}_6$, operating at a DC current density of 30 mA cm^{-2} at room temperature, was used for the Sn electrodeposition. This process provided an Sn coating with an ultrafine grain size. The electrodes produced in this way were designated as Sn–CFP. The same Sn coating with a mass loading of $1.6 \pm 0.2 \text{ mg cm}^{-2}$ (50% lower than that deposited on the CFP) was deposited on a 25 μm -thick Cu foil, using the same electrodeposition bath.

The CFP structure was studied using an inVia Renishaw micro-Raman spectrometer with a 514 nm radiation. The surface morphologies of the electrodes were studied using an FEI Quanta 200 FEG scanning electron microscope (SEM) equipped with an energy dispersive spectroscope (EDS) and a cathodoluminescence (CL) detector. To characterize the cross-sectional microstructures of the electrodes, focused ion beam (FIB) studies were carried out using a Zeiss NVision 40 dual beam SEM/FIB instrument. Using Ga-ion beam currents ranging from 13 nA to 700 pA at a voltage of 30 kV, trenches were milled across the diameter of the Sn-coated carbon fibres in their as-prepared condition and after the electrochemical experiments.

2.2. Electrochemical characterization

The electrodeposited samples were washed with distilled water and dried in 60 °C air for 5 min. The Sn–CFP sheet and the Sn-coated Cu foil were cut to a diameter of 20 mm, and the produced electrodes were weighed using an electronic balance with a sensitivity of 10 μg . The electrodes (anodes) were placed inside a CR2032-type coin cell with a 0.38 mm-thick metallic Li counter electrode and a microporous polypropylene membrane (Celgard 2400) used as the separator. The electrolyte was composed of 1 M LiPF_6 in a mixture of ethylene carbonate, dimethyl carbonate and diethylene carbonate (1:1:1 volume ratio). All cells were assembled in an MBRAUN LABstar glovebox filled with dry argon ($\text{H}_2\text{O} < 1 \text{ ppm}$, $\text{O}_2 < 1 \text{ ppm}$). Before assembling the electrochemical cells, the electrodes were dried in argon at room temperature for 3 days and washed with the electrolyte solution prior to inserting them into the cells to ensure the dryness of the cells.

Galvanostatic charge–discharge cycling tests with a voltage cut off window of 0.02–1.50 V vs. Li/Li^+ potential were applied to the cells to evaluate the cycling performance of the electrodes. The current densities used for the charge–discharge cycling of the CFP, Sn-coated Cu and Sn–CFP electrodes were about 0.75 mA cm^{-2} , 0.75 mA cm^{-2} and 1.50 mA cm^{-2} , respectively.

The active material's mass in the Sn–CFP composite electrode was calculated as:

$$M_{\text{active}} = M_{\text{Sn}} + M_{\text{C}} \quad (2)$$

where M_{Sn} was the Sn coating's mass and M_{C} was the mass of the carbon fibres participating in the lithiation/delithiation process.

After the electrochemical tests, the cycled electrodes were removed from the cell inside the glovebox and dried in argon for further microstructural investigations.

3. Results and discussion

3.1. Microstructure of fabricated electrodes

SEM micrographs of the Sn coating electrodeposited on the Cu foil substrate are presented in Fig. 1a and b. The Sn coating's surface was flat (Fig. 1a) and composed of ultrafine Sn grains with an average size of $350 \pm 50 \text{ nm}$ (Fig. 1b).

The microstructure of the Sn–CFP is shown in Fig. 2a, and a higher magnification SEM micrograph of the Sn-coated carbon fibres from the location marked as 'b' is presented in Fig. 2b. The Sn coating uniformly covered the entire surfaces of the carbon fibres in the top $65 \pm 5 \text{ }\mu\text{m}$ of the CFP's thickness ($370 \text{ }\mu\text{m}$). The coating had an ultrafine grain size of $350 \pm 50 \text{ nm}$, as seen in the higher magnification SEM micrograph displayed in Fig. 2c. A secondary electron micrograph of an Sn-coated carbon fibre's cross-section prepared by FIB is shown in Fig. 2d. This micrograph shows that the fibres were coated uniformly by Sn. The cross-sectional view of the Sn grains is also exposed; revealing only a single layer of Sn grains across the thickness of the coating. As shown in Fig. 2d the coating's thickness was $0.5 \pm 0.1 \text{ }\mu\text{m}$. Although the Sn mass loading of the Sn–CFP composite was two times more than that of the Sn-coated Cu, the Sn coating in the Sn–CFP was four times thinner than that deposited on the Cu foil ($2.2 \pm 0.2 \text{ }\mu\text{m}$), indicating that the surface-to-volume ratio of Sn in the Sn–CFP composite was four times higher. This implies that the Sn–CFP electrode would have higher chemical reactivity compared to the Sn-coated Cu, as will be described in Section 3.2.

It should also be noted that the large curvature (the amount by which the surface deviates from being flat, as defined by $\kappa = r^{-1}$, where r is the radius of a coated fibre) of the Sn coating on the carbon fibres would enhance its tolerance for volume changes.

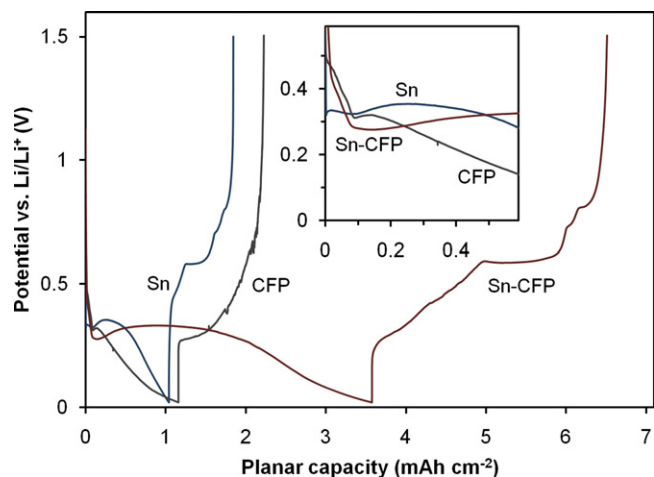


Fig. 3. Galvanostatic charge–discharge voltage profiles of the CFP, Sn-coated Cu and Sn–CFP electrodes for the first cycle.

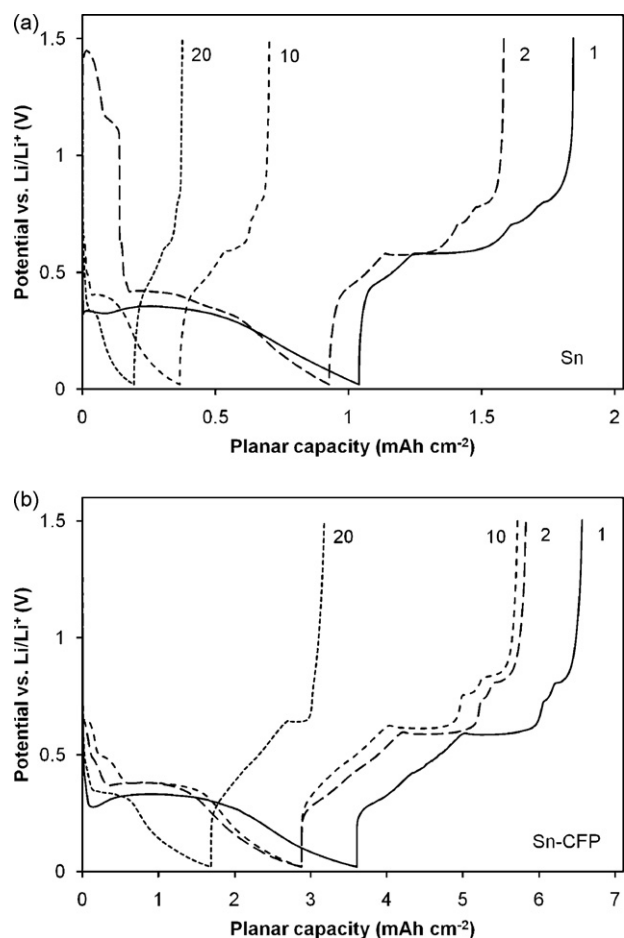


Fig. 4. Galvanostatic charge–discharge voltage profiles during the first, second, tenth and twentieth cycles for: (a) the Sn-coated Cu electrode, and (b) the Sn-CFP electrode.

3.2. Electrochemical performance

The galvanostatic charge–discharge profiles of the CFP, Sn-coated Cu and Sn-CFP electrodes recorded for the first cycle are presented in Fig. 3. The CFP's charge potential decreased gradually, rather than showing steps at low values (i.e., 0.1–0.2 V vs. Li/Li^+), which is characteristic of less ordered carbon structures compared to graphite [32]. In addition, the curvature of the charge potential was positive below 0.2 V. The CFP's discharge potential also showed a positive curvature from 0.25 V to 0.6 V. The Sn-coated Cu electrode's charge potential, in contrast, showed a potential plateau just below 0.4 V and then decreased almost linearly to 0.02 V. The electrode's discharge potential, however, surged to about 0.4 V, at which point a reduction in slope occurred with delithiation plateaus taking place between 0.6 and 0.8 V. The Sn-CFP electrode showed the lithiation/delithiation plateaus that were observed for the Sn-coated Cu, but the lithiation/delithiation curves, similar to those observed for the CFP electrode, were also observed at lower potentials. During the first charge, the lithiation of the Sn coating in the Sn-CFP electrode formed a long plateau below 0.4 V, followed by the lithiation of the carbon fibres that created a positive potential curvature below 0.2 V. During the first discharge, the delithiation of the carbon fibres started above 0.25 V, as evidenced from the gradual increase in potential from 0.25 V to 0.6 V, followed by large Sn delithiation plateaus that took place between 0.6 and 0.8 V. This suggests that both intercalation and alloying mechanisms were active in the Sn-CFP electrode.

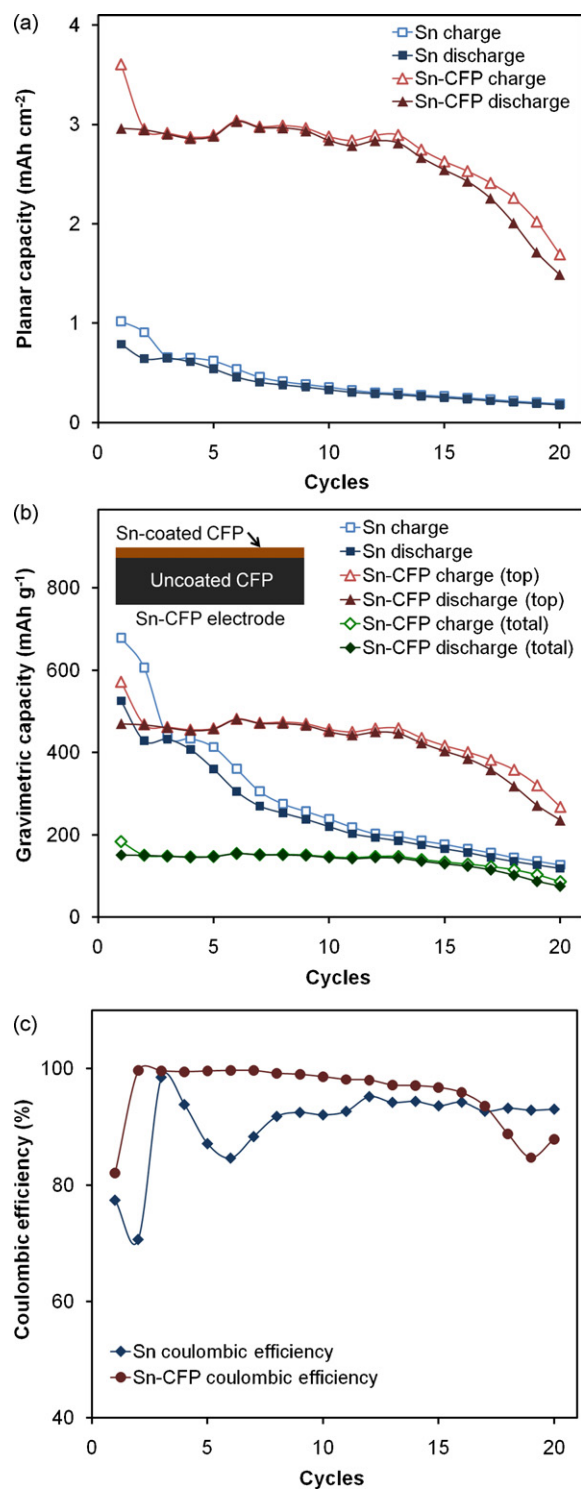


Fig. 5. Capacities and efficiencies of the Sn-coated Cu and the Sn-CFP electrodes. (a) Planar charge–discharge capacities. (b) Gravimetric charge–discharge capacities. (c) Coulombic efficiencies.

The galvanostatic charge–discharge profiles of the Sn-coated Cu and the Sn-CFP electrodes for the first, second, tenth and twentieth cycles are presented in Fig. 4a and b. The planar capacities of both electrodes declined from the first cycle to the twentieth cycle, 78% with the Sn-coated Cu and 50% with the Sn-CFP electrode. It should also be noted that the Sn-coated Cu electrode displayed an irreversible high-voltage capacity (i.e., 1.4–1.1 V vs. Li/Li^+) during the second charge (Fig. 4a); a phenomenon that was not observed in

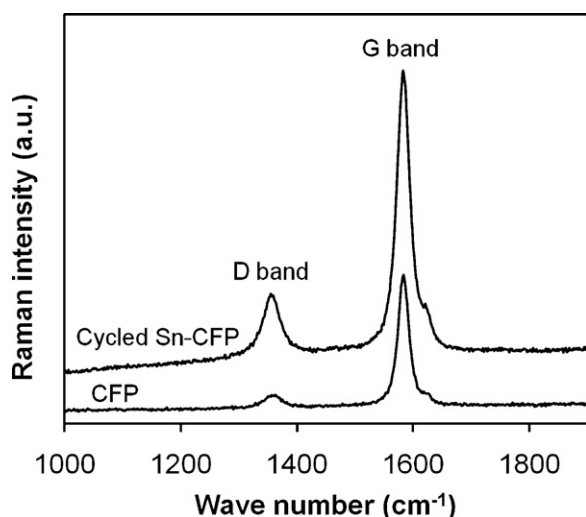


Fig. 6. Micro-Raman spectra of the carbon fibres in the as-received CFP and the Sn-CFP electrode after twenty galvanostatic charge-discharge cycles.

the Sn-CFP electrode's charge profiles (Fig. 4b). This phenomenon, which is due to the irreversible reaction of Li^+ ions with Sn oxides (e.g., SnO) and formation of Li_2O particles on the surface of the Sn coating, resulted in a low Coulombic efficiency of 71% for the second cycle, compared to an efficiency of 100% calculated for the Sn-CFP electrode during the same cycle.

The planar charge-discharge capacities of the Sn-coated Cu and the Sn-CFP electrodes are plotted in Fig. 5a. For the first cycle, the planar discharge capacity of the Sn-CFP electrode was 2.96 mAh cm^{-2} , almost four times higher than that of the Sn-coated Cu (0.79 mAh cm^{-2}). The capacity of the Sn-coated Cu continuously declined with almost every cycle. The Sn-CFP electrode's capacity did not show a significant decline for the first fifteen cycles, but rather displayed a capacity retention of 86% compared to the 32% measured for the Sn-coated Cu electrode. For the twentieth

Table 1

Comparison of the planar capacities and Coulombic efficiencies of the Sn-CFP and the Sn-coated Cu electrodes for the first, second, tenth and twentieth charge-discharge cycles.

Cycle No.	Planar Capacity (mAh cm^{-2})		Coulombic efficiency (%)	
	Sn-CFP	Sn	Sn-CFP	Sn
1	2.96	0.79	82	77
2	2.95	0.64	100	71
10	2.84	0.33	99	92
20	1.49	0.18	88	93

cycle, the planar capacity of the Sn-CFP electrode (1.49 mAh cm^{-2}) was more than eight times higher than that of the Sn-coated Cu electrode (0.18 mAh cm^{-2}).

The gravimetric charge-discharge capacities of the Sn-coated Cu and the Sn-CFP electrodes are plotted in Fig. 5b. As shown in the schematic drawing of the Sn-CFP electrode (see the inset of Fig. 5b), the Sn-CFP electrode could be divided into two distinct layers along its thickness. The top layer is a Sn-carbon fibre composite layer that contains about 18% of the total mass of the CFP. The carbon fibres below this top layer could not be reached by Sn^{2+} ions, and hence, they form an uncoated CFP layer. The gravimetric capacities of the Sn-CFP electrode are represented by two distinct curves in Fig. 5b. The first curve, designated as 'top', represents the gravimetric capacities that were calculated by taking into account only the top layer's mass as the active material's mass in Eq. (2), while the second curve, designated as 'total', represents the gravimetric capacities that were calculated by taking into account the Sn-CFP electrode's total mass as the active material's mass. In the first cycle, the gravimetric discharge capacity for the Sn-CFP electrode's top layer was 470 mAh g^{-1} (152 mAh g^{-1} for the Sn-CFP electrode's total mass), compared to 526 mAh g^{-1} for the Sn-coated Cu electrode. In the twentieth cycle, the capacity for the Sn-CFP electrode's top layer was 236 mAh g^{-1} (76 mAh g^{-1} for the Sn-CFP electrode's total mass), compared to 118 mAh g^{-1} for the Sn-coated Cu electrode.

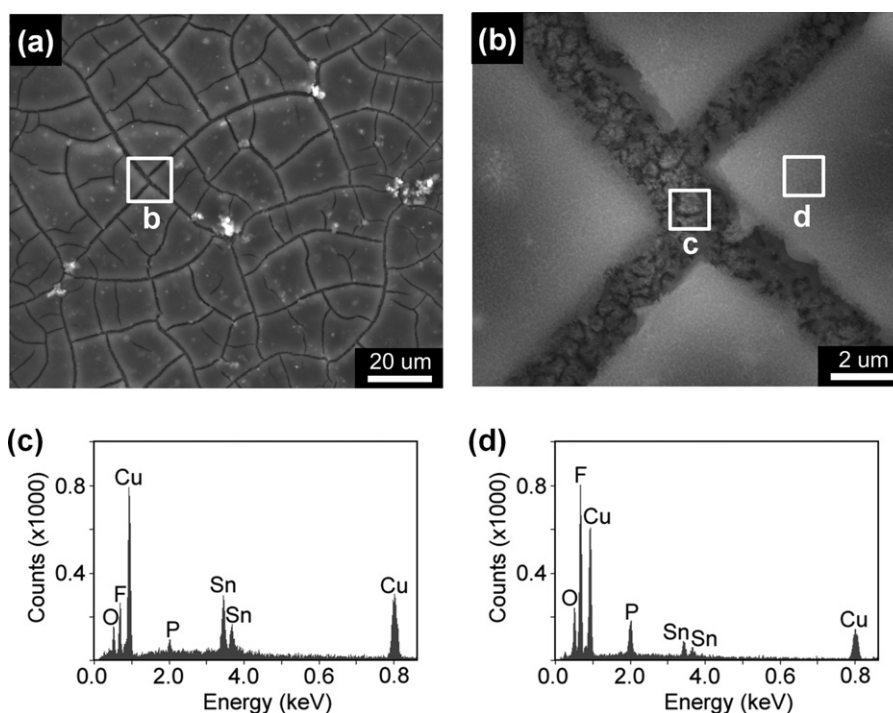


Fig. 7. (a and b) SEM (secondary electron) micrographs of the Sn-coated Cu electrode after twenty galvanostatic charge-discharge cycles, and (c and d) EDS spectra of the intersection of four patches as shown in (b).

The Coulombic efficiencies of the Sn-coated Cu and the Sn-CFP electrodes are plotted in Fig. 5c. The Coulombic efficiency of the Sn-CFP electrode was higher and more stable than that of the Sn-coated Cu electrode. For the first cycle, the efficiencies of the Sn-coated Cu and the Sn-CFP electrodes were 77% and 82%, respectively. The low efficiencies in the first cycle are attributed largely to irreversible reactions with the electrolyte that form a solid electrolyte interphase (SEI) layer on the active material. After the first

cycle, the Sn-CFP electrode's efficiency increased to 100% for the second cycle and stayed above 95% for most of the remaining cycles, whereas it took the Sn-coated Cu seven cycles to stabilize and reach an efficiency above 90%.

A comparison of the planar capacities and Coulombic efficiencies of the Sn-CFP and the Sn-coated Cu electrodes during the first, second, tenth and twentieth charge–discharge cycles is presented in Table 1.

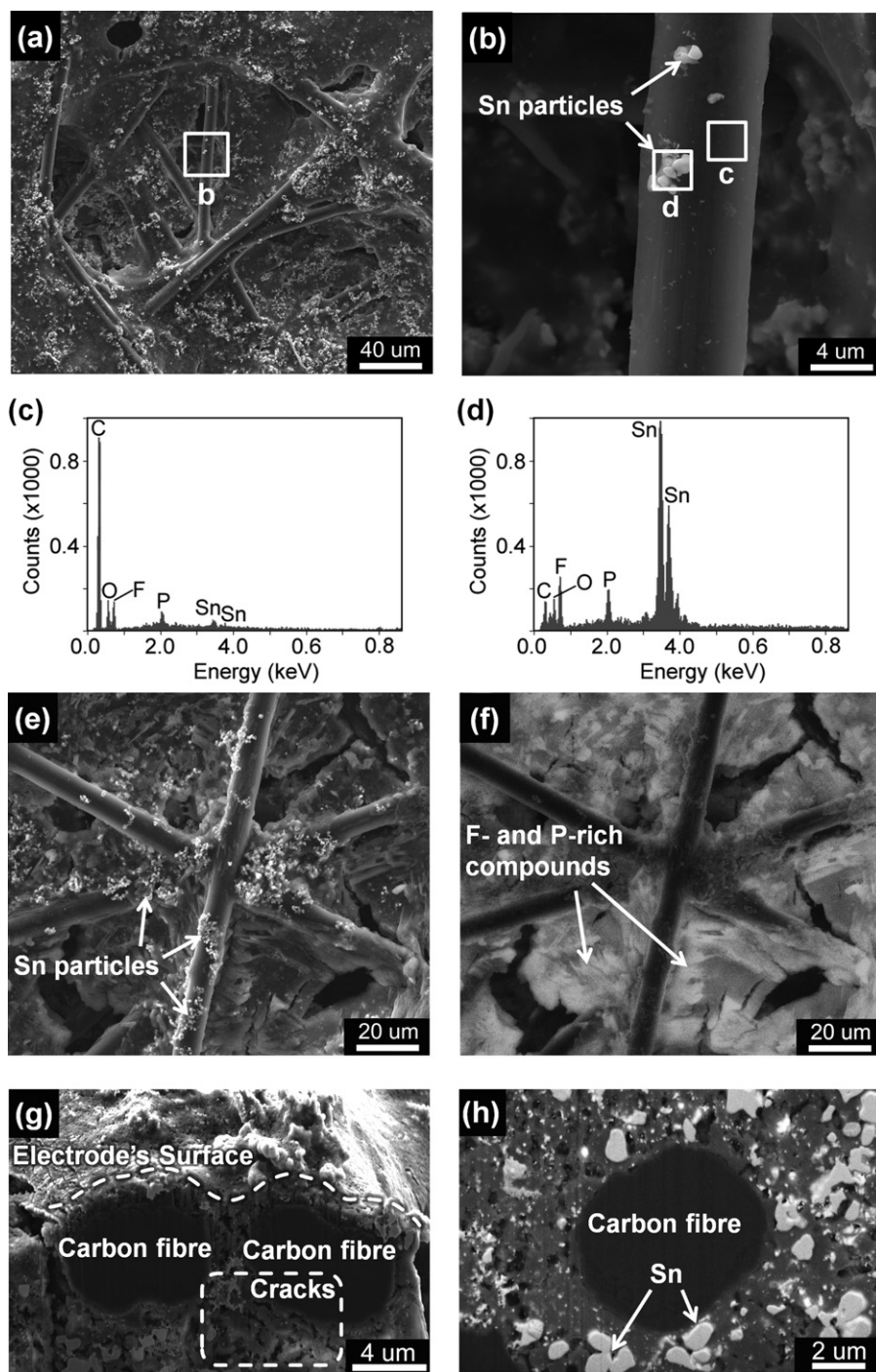


Fig. 8. SEM micrographs of the Sn-CFP electrode after twenty galvanostatic charge–discharge cycles: (a) secondary electron micrograph of Sn-CFP microstructure, (b) secondary electron micrograph of a carbon fibre at a higher magnification, (c and d) EDS spectra of the carbon fibre as shown in (b), (e) Secondary electron micrograph of intersection of three carbon fibres in the Sn-CFP electrode, (f) cathodoluminescence micrograph of the area shown in (e) revealing F- and P-rich compounds, (g) secondary electron micrograph of an FIB-milled cross section of two carbon fibres lying under the surface of the cycled Sn-CFP electrode, and (h) back-scattered electron micrograph of the cross section of a carbon fibre buried under the electrode's surface.

3.3. Microscopical evaluation of the electrochemical degradation

The micro-Raman spectra of the carbon fibres in the as-received CFP sheet and the Sn–CFP electrode after twenty charge–discharge cycles are presented in Fig. 6, showing distinct peaks at 1360 and 1582 cm^{-1} that correspond to the D and G bands of sp^2 -bonded carbon, respectively [33]. The presence of the D band and the peak intensity ratio I_D/I_G indicate that the as-received CFP had some microstructural disorder, possibly due to the presence of exposed edge planes along each fibre [34]. The charge–discharge cycling increased the peak intensity ratio I_D/I_G from 0.19 to 0.36, indicating that severe structural damage was inducted into the carbon fibres during electrochemical cycling [35,36]. This confirms that the intercalation mechanism was active in the Sn–CFP electrode, along with the alloying mechanism.

After twenty galvanostatic charge–discharge cycles, a network of microscopic cracks was observed on the surface of the Sn-coated Cu electrode, creating patches with different sizes and shapes on the surface that resembled typical “mud cracks,” as shown in Fig. 7a. The “mud crack” morphology formed as the result of large volume changes induced by the lithiation/delithiation processes. A higher magnification micrograph taken from the region labeled as ‘b’ in this micrograph is shown in Fig. 7b, and reveals that cracks as wide as 2 μm were formed. The EDS analyses of areas ‘c’ and ‘d’ shown in Fig. 7b are presented in Fig. 7c and d. The signal intensities of Sn (from the coating) and Cu (from the substrate) measured inside the cracks were higher than those measured on the patches between the cracks, but the patches were rich in F and P. This suggests that the surface of the Sn-coated Cu electrode could be covered by the electrolyte residues and SEI layers.

SEM micrographs in Fig. 8 display the microstructure of the Sn–CFP electrode that was examined after twenty galvanostatic charge–discharge cycles. The secondary electron micrograph of the Sn–CFP electrode is shown in Fig. 8a. Compared to the original, as-prepared morphology (Fig. 2a), the cycled Sn–CFP electrode was less porous, and the carbon fibres seemed to be embedded in a translucent matrix. No evidence of notable disintegration or fracture could be found on the Sn–CFP electrode’s surface (Fig. 8a). A secondary electron micrograph of a carbon fibre taken from the region labeled as ‘b’ and observed at a higher magnification (Fig. 8b) revealed that the carbon fibre’s surface was covered by a continuous layer and some fine Sn particles. The EDS spectra of the carbon fibre shown in Fig. 8b are presented in Fig. 8c and d, revealing that the layer covering the carbon fibre was rich in F and P (i.e., an SEI layer). Fig. 8e shows the contact junction made by three intersecting carbon fibres. These intersections were frequent, and indicate that carbon fibres formed “bridges” through which the electrical conductivity of the electrode was maintained in different directions. A cathodoluminescence micrograph of the area shown in Fig. 8e is presented in Fig. 8f, and indicates the presence of a thick layer containing F and P (white) in the areas between the carbon fibres (black), compared to the thin layer observed on the carbon fibres (see Fig. 8b and c).

An FIB-milled cross section showing two carbon fibres lying under the surface of the cycled Sn–CFP electrode is presented in Fig. 8g, while a back-scattered electron micrograph of the cross section of a carbon fibre buried under the surface appears in Fig. 8h. The matrix surrounding carbon fibres composed of F- and P-rich compounds containing Sn particles ranging from about 1 μm to a few nanometers in diameter, and a network of microcracks around the fibres could have been formed as the result of the large volume changes during the charge–discharge cycles. However, the fibres were still connected to the surrounding matrix after twenty cycles.

Generally, large volume changes during electrochemical cycling form unstable interfaces with the electrolyte that may quickly deteriorate electrode’s performance. The aforementioned observations

of the Sn–CFP electrode’s damaged microstructure indicate that during the charge–discharge cycling the Sn coating’s particles were detached from the carbon fibres, forming a thick film composed of Sn nanoparticles, electrolyte residues and SEI layers that filled the microscopic pores between the carbon fibres. Although the new composite was still well connected through a network of randomly oriented carbon fibres, the short-range connection between the Sn particles and the carbon fibres was undermined, contributing to a gradual decrease in the energy storage capacity of the Sn–CFP electrode after fifteen cycles (Fig. 5a and b).

It is likely that a heat treatment process may enhance the cycling performance of the composite electrode by: (i) improving the bond between the Sn coating and the carbon fibres, delaying the detachment of the Sn particles from carbon fibres’ surfaces that may reduce the growing rate of the film composed of Sn particles, electrolyte residues and SEI layers; or (ii) transforming Sn to Sn oxides (if heat treated in the presence of O_2) that could irreversibly react with Li^+ ions and convert to metallic Sn particles finely dispersed in a Li_2O matrix during the first charge in a Li cell. The Li_2O matrix conducts Li^+ ions and accommodates the mechanical stresses caused by lithiation/delithiation of the Sn particles during the subsequent cycles [37,38]. The SnO_x -CFP electrodes produced from heat treating Sn–CFP composites may be good alternatives to commercial graphitic anodes for cost-effective, rechargeable Li-ion batteries with high capacity and good cycle life.

4. Conclusions

An ultrafine grain ($350 \pm 50 \text{ nm}$) Sn coating with a thickness of $0.5 \pm 0.1 \mu\text{m}$ was electrodeposited on the randomly oriented fibres of a carbon fibre paper (CFP) to produce an Sn–carbon fibre composite anode for rechargeable Li-ion batteries. Galvanostatic charge–discharge tests conducted by using relatively large current densities showed that the Sn–CFP electrode had a reversible planar capacity of 2.96 mAh cm^{-2} with a capacity retention of 50% after twenty cycles, compared to the 23% measured for a $2.2 \pm 0.2 \mu\text{m}$ thick Sn coating deposited on a Cu foil. The higher capacity retention of the Sn–CFP electrode was attributed to the following factors:

- (i) The small thickness and large surface area of the Sn coating on the carbon fibres boosted the coating’s chemical reactivity and tolerance for volume change.
- (ii) In addition to acting as randomly oriented current collectors, carbon fibres participated in lithiation/delithiation processes as active materials, boosting the cell’s overall performance and stability.

Acknowledgements

Financial support for this study was provided by the Natural Sciences and Engineering Research Council of Canada (NSERC). The authors are grateful of Dr. R. Aroca of the University of Windsor for the micro-Raman spectrometry tests. The authors would also like to thank Dr. G. de Silveira and Ms. J. Huang from the Canadian Centre for Electron Microscopy (CEEM) for their assistance with the FIB microscopy.

References

- [1] S. Megahed, B. Scrosati, J. Power Sources 51 (1994) 79–104.
- [2] R. Moshkev, B. Johnson, J. Power Sources 91 (2000) 86–91.
- [3] B. Scrosati, Electrochim. Acta 45 (2000) 2461–2466.
- [4] J.M. Tarascon, M. Armand, Nature 414 (2001) 359–367.
- [5] D. Larcher, S. Beattie, M. Morcrette, K. Edstrom, J.C. Jumas, J.M. Tarascon, J. Mater. Chem. 17 (2007) 3759–3772.

- [6] A. Anani, S. Crouch-Baker, R.A. Huggins, J. Electrochem. Soc. 134 (1987) 3098–3102.
- [7] K.D. Kepler, J.T. Vaughey, M.M. Thackeray, Electrochem. Solid State Lett. 2 (1999) 307–309.
- [8] A. Magasinski, P. Dixon, B. Hertzberg, A. Kvit, J. Ayala, G. Yushin, Nat. Mater. 9 (2010) 353–358.
- [9] H. Zhao, C. Jiang, X. He, J. Ren, C. Wan, Ionics 14 (2008) 113–120.
- [10] P. Limthongkul, H. Wang, Y.-M. Chiang, Chem. Mater. 13 (2001) 2397–2402.
- [11] J.-H. Ahn, G.X. Wang, J. Yao, H.K. Liu, S.X. Dou, J. Power Sources 119–121 (2003) 45–49.
- [12] C.R. Sides, N. Li, C.J. Patrissi, B. Scrosati, C.R. Martin, MRS Bull. 27 (2002) 604–607.
- [13] C.K. Chan, H. Peng, G. Liu, K. Mcllwraith, X.F. Zhang, R.A. Huggins, Y. Cui, Nat. Nanotechnol. 3 (2008) 31–35.
- [14] M. Winter, J.O. Besenhard, Electrochim. Acta 45 (1999) 31–50.
- [15] M. Wachtler, J.O. Besenhard, M. Winter, J. Power Sources 94 (2001) 189–193.
- [16] M. Wachtler, M. Winter, J.O. Besenhard, J. Power Sources 105 (2002) 151–160.
- [17] I.A. Courtney, J.R. Dahn, J. Electrochem. Soc. 144 (1997) 2045–2052.
- [18] K.D. Kepler, J.T. Vaughey, M.M. Thackeray, J. Power Sources 81–82 (1999) 383–387.
- [19] S.D. Beattie, J.R. Dahn, J. Electrochem. Soc. 150 (2003) A894–A898.
- [20] W. Choi, J.Y. Lee, H.S. Lim, Electrochem. Commun. 6 (2004) 816–820.
- [21] N. Tamura, A. Fujimoto, M. Kamino, S. Fujitani, Electrochim. Acta 49 (2004) 1949–1956.
- [22] J. Chen, S.J. Bull, S. Roy, H. Mukaibo, H. Nara, T. Momma, T. Osaka, Y. Shacham-Diamand, J. Phys. D: Appl. Phys. 41 (2008) 025302.
- [23] H. Mukaibo, T. Sumi, T. Yokoshima, T. Momma, T. Osaka, Electrochem. Solid State Lett. 6 (2003) A218–A220.
- [24] J. Hassoun, S. Panero, B. Scrosati, J. Power Sources 160 (2006) 1336–1341.
- [25] M. Noh, Y. Kwon, H. Lee, J. Cho, Y. Kim, M.G. Kim, Chem. Mater. 17 (2005) 1926–1929.
- [26] J.W. Park, J.Y. Eom, H.S. Kwon, Electrochem. Commun. 11 (2009) 596–598.
- [27] L. Trahey, J.T. Vaughey, H.H. Kung, M.M. Thackeray, J. Electrochem. Soc. 156 (2009) A385–A389.
- [28] L. Huang, H.B. Wei, F.S. Ke, X.Y. Fan, J.T. Li, S.G. Sun, Electrochim. Acta 54 (2009) 2693–2698.
- [29] T. Jiang, S. Zhang, X. Qiu, W. Zhu, L. Chen, J. Power Sources 166 (2007) 503–508.
- [30] L. Bazin, S. Mitra, P.L. Taberna, P. Poizot, M. Gressier, M.J. Menu, A. Barnabe, P. Simon, J.M. Tarascon, J. Power Sources 188 (2009) 578–582.
- [31] C. Arbizzani, S. Beninati, M. Lazzari, M. Mastragostino, J. Power Sources 141 (2005) 149–155.
- [32] J.O. Besenhard, J. Yang, M. Winter, J. Power Sources 68 (1997) 87–90.
- [33] A.C. Ferrari, J. Robertson, Phys. Rev. B61 (2000) 14095–14107.
- [34] A.E. Fischer, M.A. Lowe, G.M. Swain, J. Electrochem. Soc. 154 (2007) K61–K67.
- [35] L.J. Hardwick, P.W. Ruch, M. Hahn, W. Scheifele, R. Kotz, P. Novak, J. Phys Chem. Solids 69 (2008) 1232–1237.
- [36] V.A. Sethuraman, L.J. Hardwick, V. Srinivasan, R. Kostecki, J. Power Sources 195 (2010) 3655–3660.
- [37] Y. Idota, T. Kubota, A. Matsufuji, Y. Maekawa, T. Miyasaka, Science 276 (1997) 1395–1397.
- [38] S. D'Andrea, S. Panero, P. Reale, B. Scrosati, Ionics 6 (2000) 127–132.